Electronic Supplementary Material (ESI) for RSC Advances.

Dental lessons from past to present: ultrastructure and composition of teeth from plesiosaurs, dinosaurs, extinct and recent sharks

Alwina Lübke, Joachim Enax, Kateryna Loza, Oleg Prymak, Peter Gaengler, Helge-Otto Fabritius, Dierk Raabe, and Matthias Epple

Supplementary information

Ultrastructural characterization of fossil and recent teeth from sharks, plesiosaurs and dinosaurs

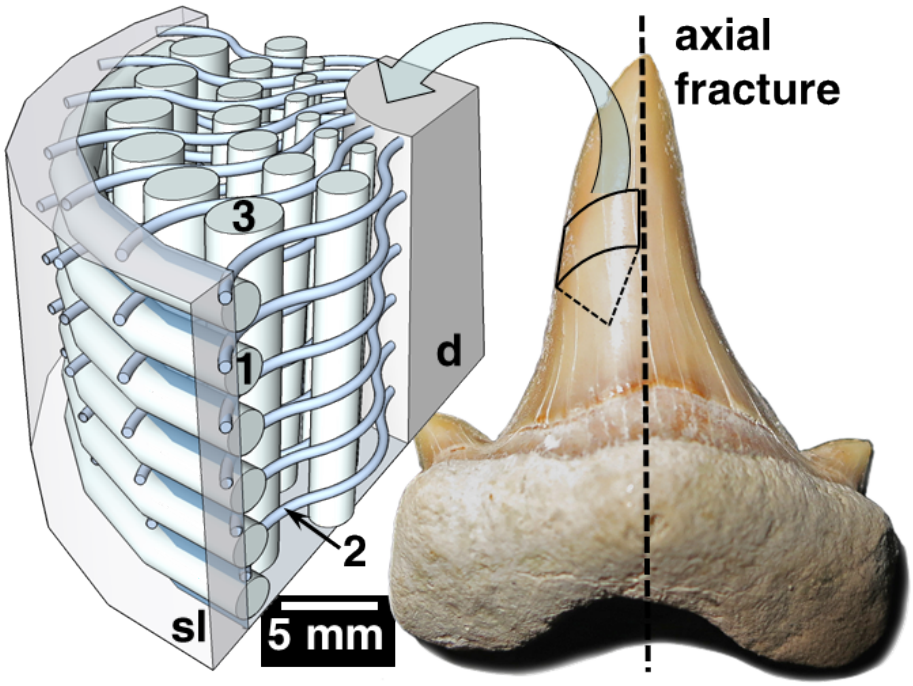

Fig. S1: Schematic depiction of sample geometry and orientation obtained by an axial fracture of the investigated teeth, demonstrating the orientation of the fluoroapatite crystallites visible on the exposed surfaces of the shark teeth. In the reptilian teeth, all crystallites are oriented perpendicularly to the tooth surface. (sl: shiny layer, d: dentin, 1: circumferential bundle, 2: radial bundle, 3: axial bundle).

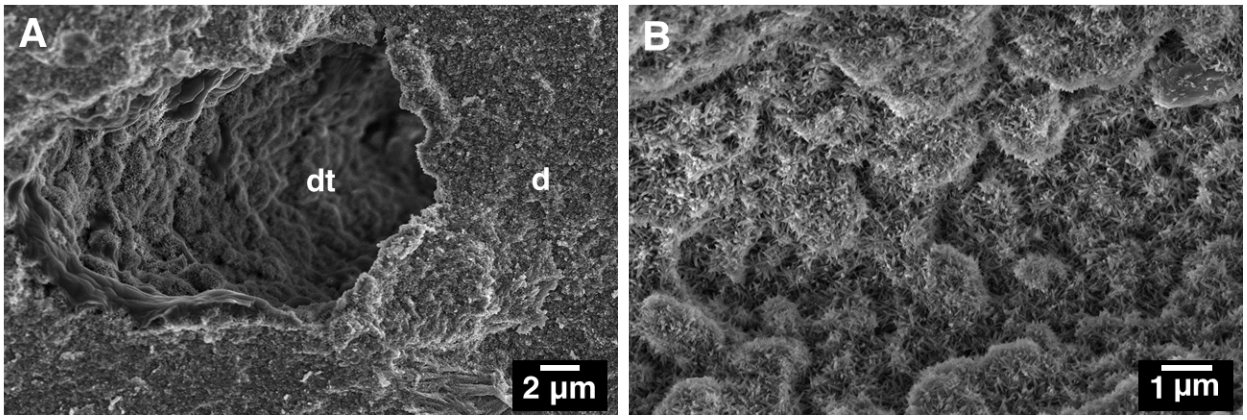

Fig. S2: Scanning electron micrographs of dentin from a fossilized tooth of the extinct shark *S. pristodontus.* (A) Nanocrystalline dentin with the exposed cavity of a tubule whose walls are covered with crystalline artefacts from diagenesis. (B) Detailed image of the tubule wall covered with spherular agglomerations of nanoscopic needle-shaped crystalline structures (d: dentin, dt: dentin tubule).

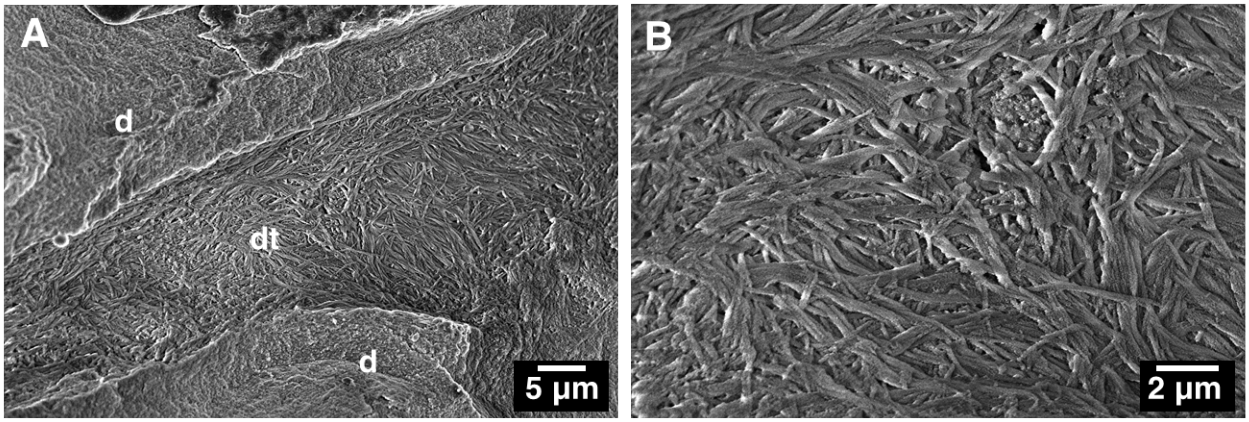

Fig. S3: Scanning electron micrographs of dentin from a fossilized tooth of the extinct shark *O. obliquus.* (A) Nanocrystalline dentin with the exposed cavities of dentin tubules whose walls are covered with artefacts from diagenesis. (B) Detailed image of the tubule wall, consisting of entangled fibrillar structures (d: dentin, dt: dentin tubule).

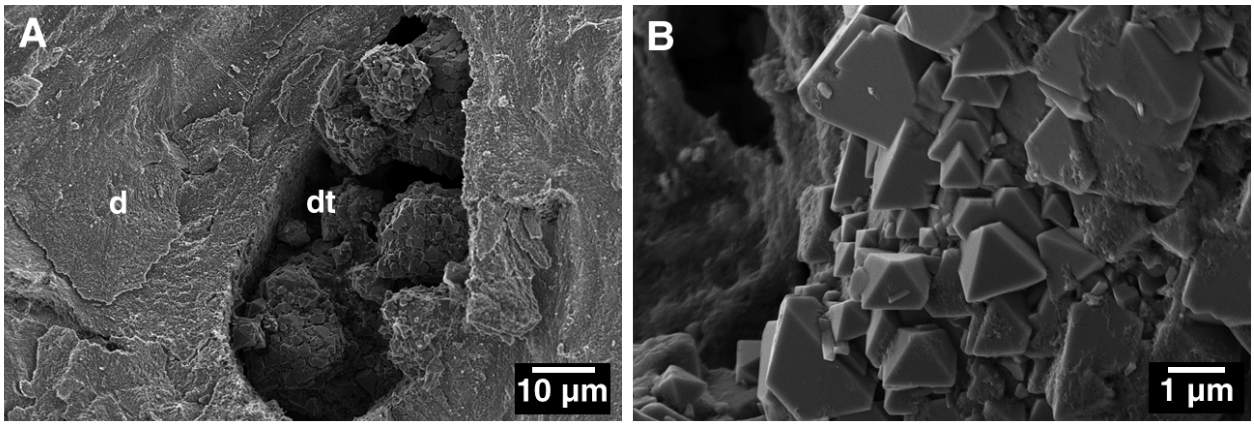

Fig. S4: Scanning electron micrographs of dentin from a fossilized tooth of the extinct shark *Carcharocles angustidens* showing artefacts from diagenesis. (A) Nanocrystalline dentin with the exposed cavity of a tubule, filled with crystalline artefacts from diagenesis. (B) Detailed image of the tubule content, consisting of large, mostly pyramid-shaped crystalline structures (d: dentin, dt: dentin tubule).

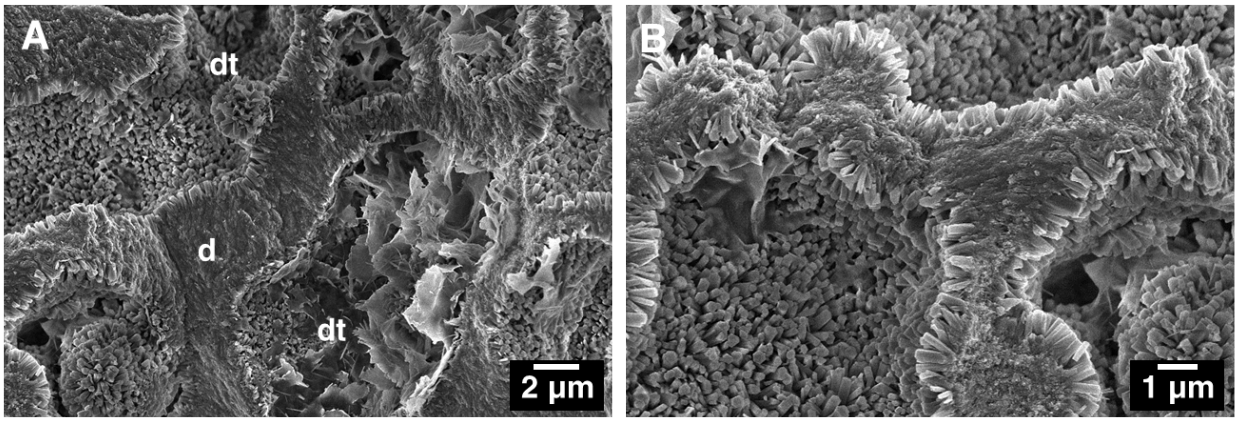

Fig. S5: Scanning electron micrographs of dentin from a fossilized tooth of the extinct shark *C. megalodon* showing artefacts from diagenesis. (A) Nanocrystalline dentin with the exposed cavities of large tubules with crystalline artefacts from diagenesis. (B) Detailed image of the tubule walls, consisting of a layer of parallel, about 500 nm thick and 1 µm long crystallites that have presumably grown towards the lumen during diagenesis (d: dentin, dt: dentin tubule).

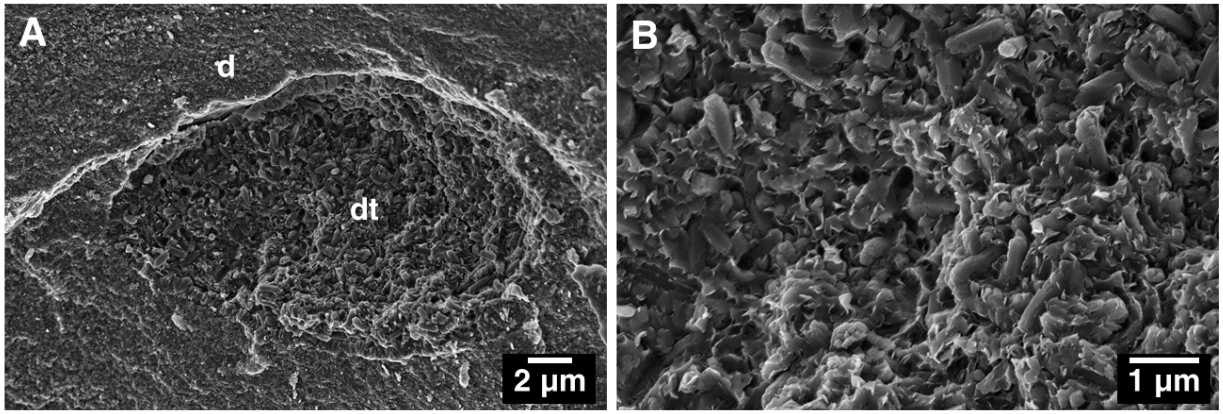

Fig. S6: Scanning electron micrographs of dentin from a fossilized tooth of the extinct shark *Isurus hastalis* with artefacts from diagenesis. (A) Nanocrystalline dentin with the exposed cavity of a tubule filled with crystalline artefacts from diagenesis. (B) Detailed image of the tubule content, consisting of a mixture of short, stubby crystallites embedded in a nanocrystalline matrix (d: dentin, dt: dentin tubule).

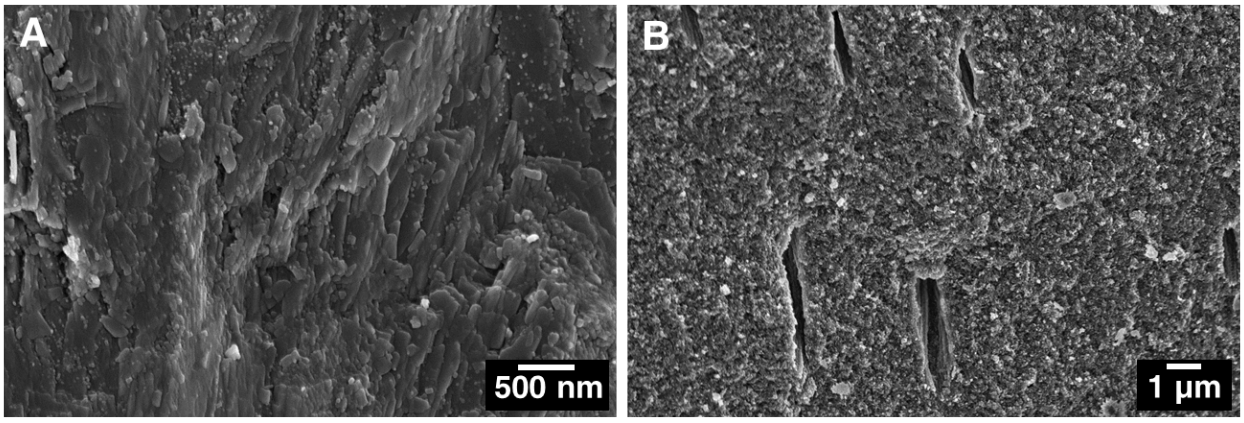

Fig. S7: Scanning electron micrographs of an axially fractured tooth of the plesiosaur *Plesiosaurus mauretanicus*: (A) Enamel with crystallites and (B) dentin with exposed tubuli.

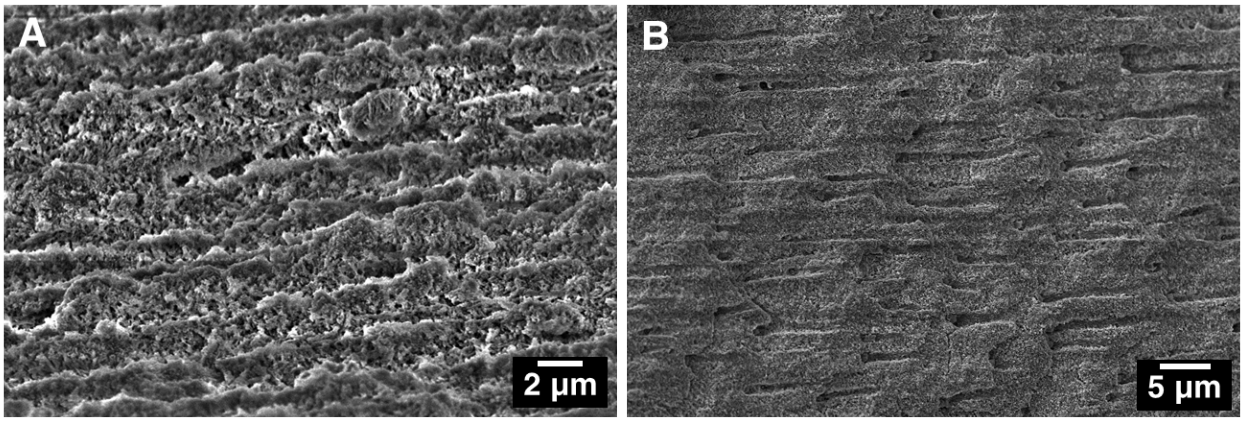

Fig. S8: Scanning electron micrographs of an axially fractured tooth of the dinosaur *Carcharodontosaurus saharicus*: (A) Enamel with crystallites and (B) dentin with exposed tubuli.

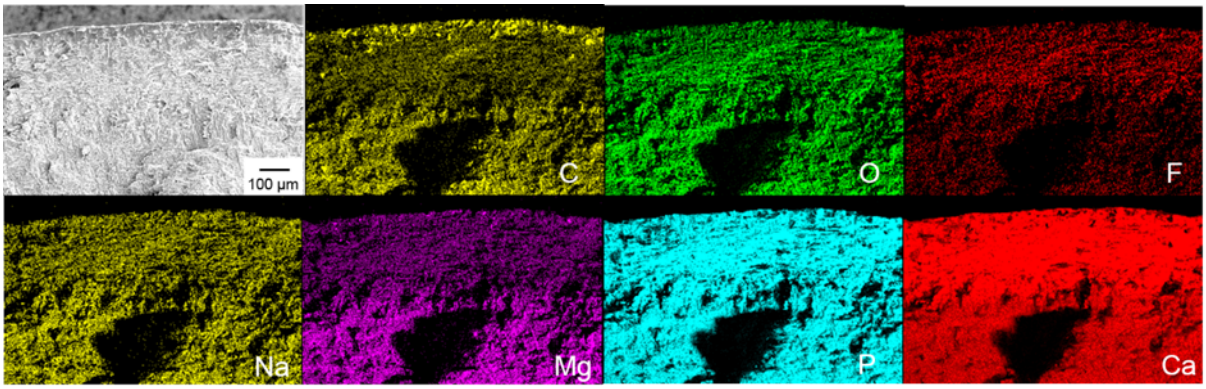

Fig. S9: Qualitative EDX mappings recorded on an axially fractured area of a tooth of *C. carcharias*, showing the distribution of C, Mg, Na, Ca, P and F. In all images enameloid is positioned above and dentin below, respectively. C, Na, and Mg are enriched in dentin whereas F and Ca are enriched in enameloid. The distribution of O and P is almost uniform. Those results are supported by the EDX line scan in Fig. S10 as well as by the chemical fluorine analysis in Table 1.

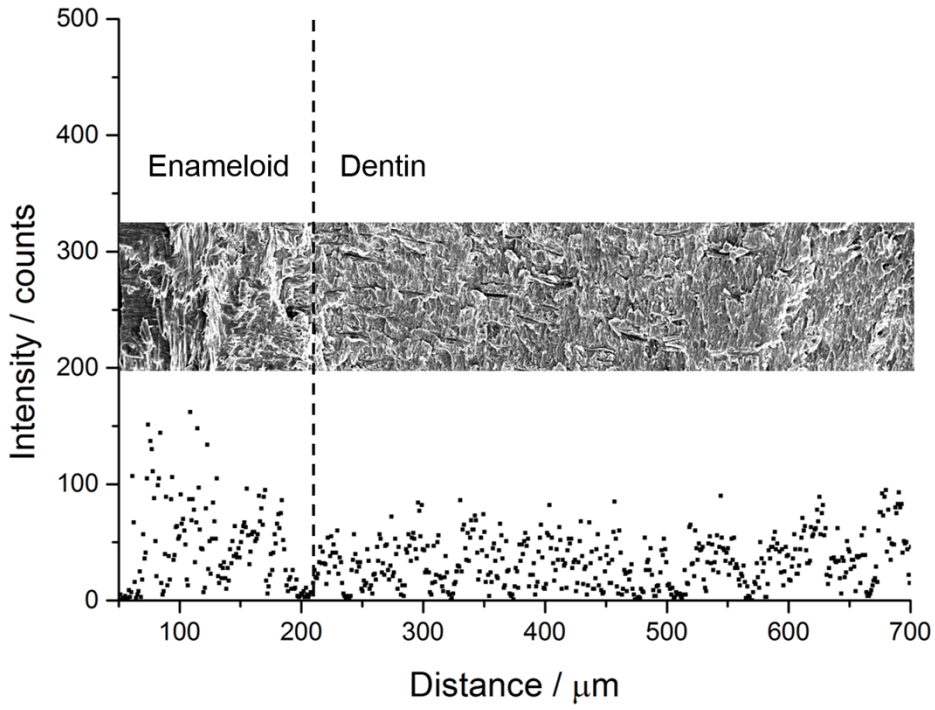

Fig. S10: Qualitative EDX line scan for fluorine as a function of the distance to the tooth surface, recorded on an axially fractured area of a tooth of *C. carcharias*, showing the content of fluoride in enameloid (slightly higher) and dentin (slightly lower).

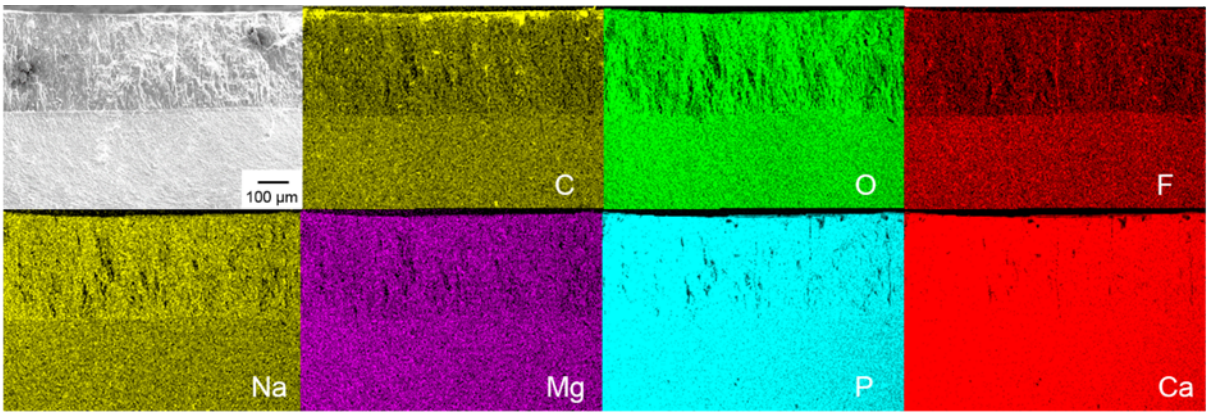

Fig. S11: Qualitative EDX mappings recorded on an axial section of a tooth of *M. beaugei*, showing the distribution of C, Mg, Na, Ca, P and F. In all images the enamel is positioned above and the dentin below, respectively. The fluorine content appears slightly lower in enameloid which is supported by the EDX line scan in Fig. S12 as well as by the chemical fluorine analysis in Table 1.

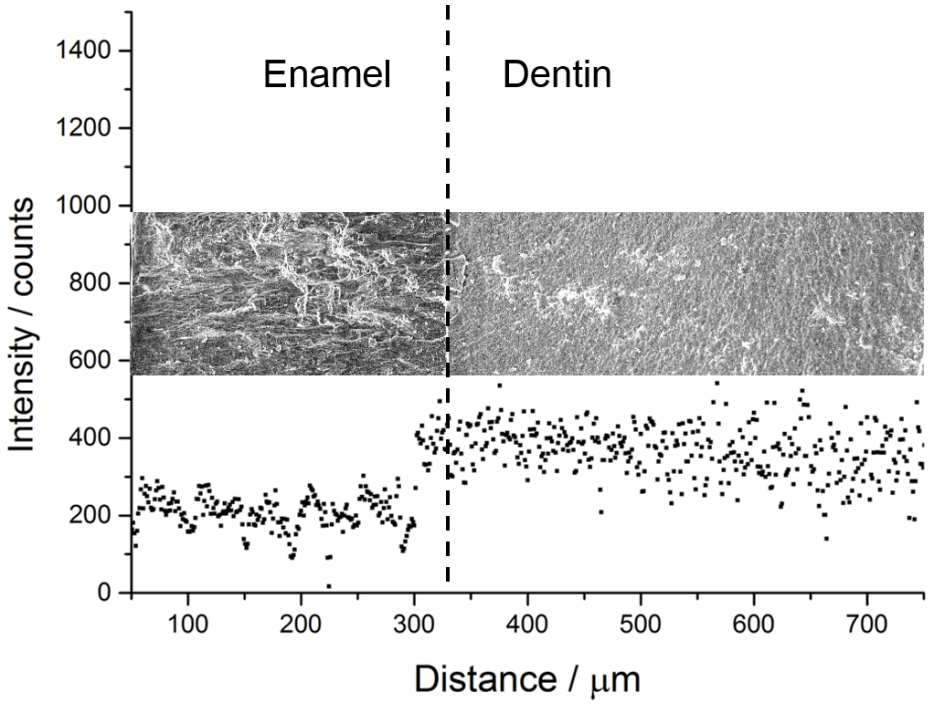

Fig. S12: Qualitative EDX line scan for fluorine as a function of the distance to the tooth surface, recorded on an axial section of a tooth of *M. beaugei*, showing the content of fluoride in the enamel (lower) and the dentin (higher).

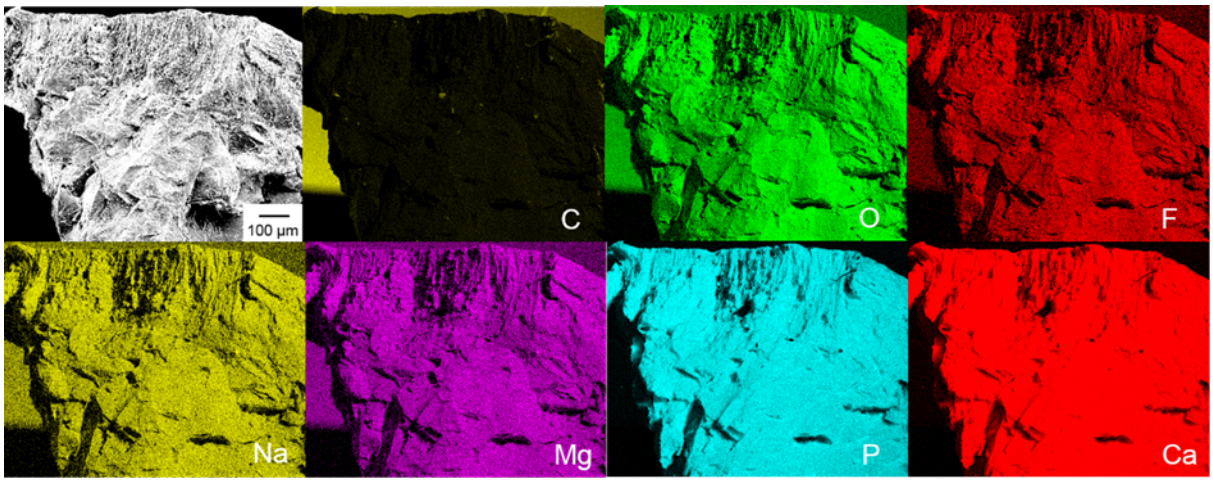

Fig. S13: Qualitative EDX mappings recorded on an axial section of a tooth of *S. pristodontus*, showing the distribution of C, Mg, Na, Ca, P and F. In all images the enamel is positioned above and the dentin below, respectively. These results are underlined by the EDX line scan in Fig. 14 as well as by the chemical fluorine analysis Table 1.

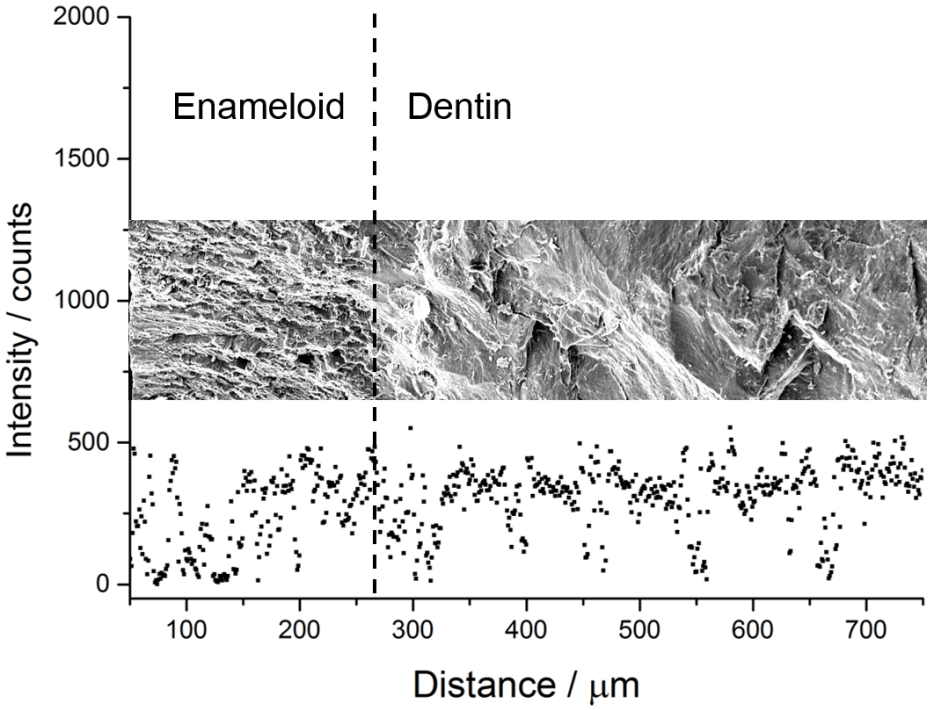

Fig. S14: Qualitative EDX line scan for fluorine as a function of the distance to the tooth surface, recorded on an axial section of a tooth of *S. pristodontus*, showing the almost identical content of fluoride in enamel and dentin.

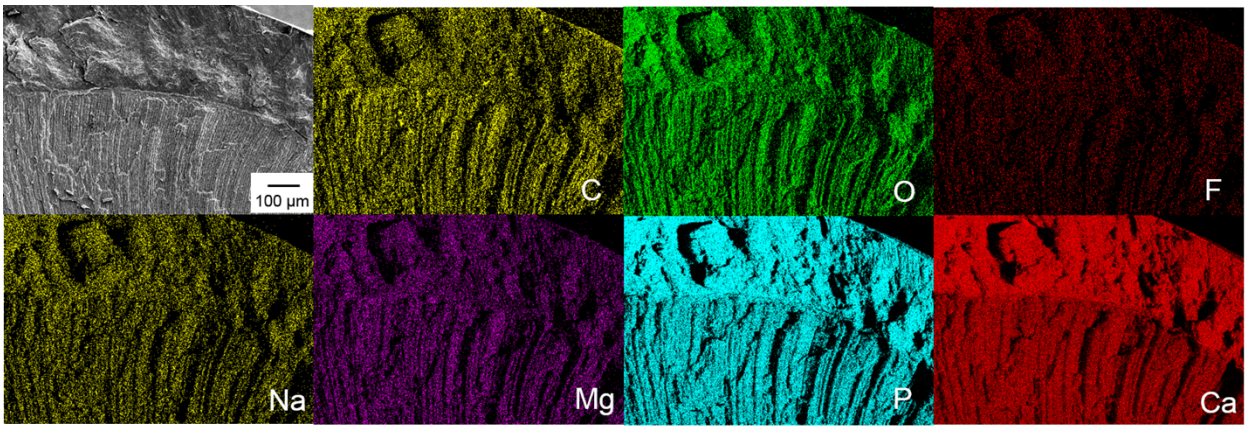

Fig. S15: Qualitative EDX mappings recorded on an axial section of a tooth of human deciduous tooth, showing the distribution of C, Mg, Na, Ca, P and F. In all images the enamel is positioned above and the dentin below, respectively. C, Na, and Mg are enriched in dentin whereas Ca is enriched in enameloid. As expected the tooth contains virtually no fluorine. The distribution of O and P is almost uniform. In case of fluorine these results are underlined by the EDX line scan in Fig. 16 as well as by the chemical fluorine analysis in Table 1.

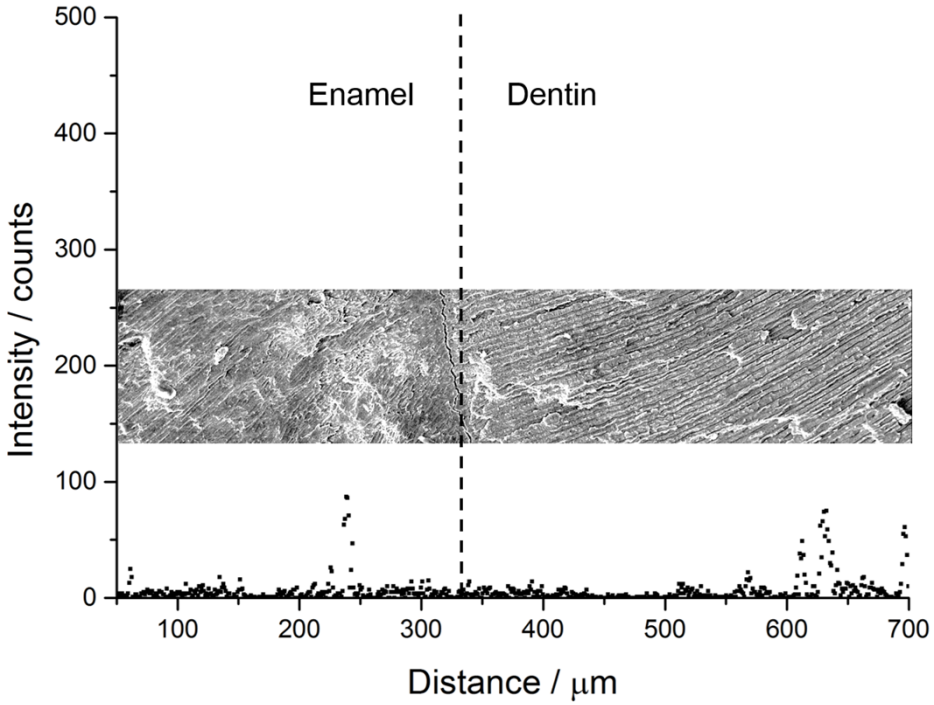

Fig. S16: Qualitative EDX line scan for fluorine as a function of the distance to the tooth surface recorded on an axial section of a human deciduous tooth, showing the almost negligible content of fluoride in enamel and dentin.

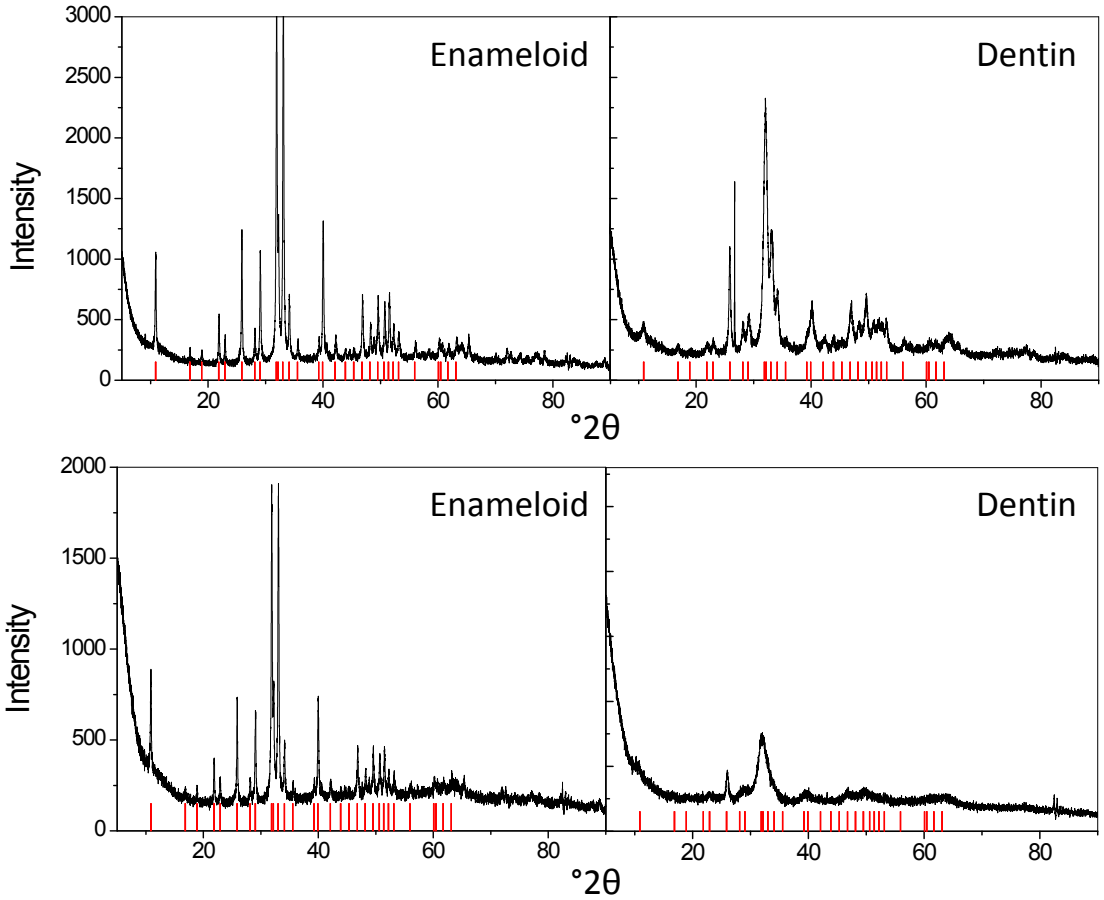

Fig. S17: X-ray powder diffractograms of the tooth of the extinct shark *C. megalodon* (top) and of the recent shark *C. carcharias* (bottom) (with reference peak positions for apatite).

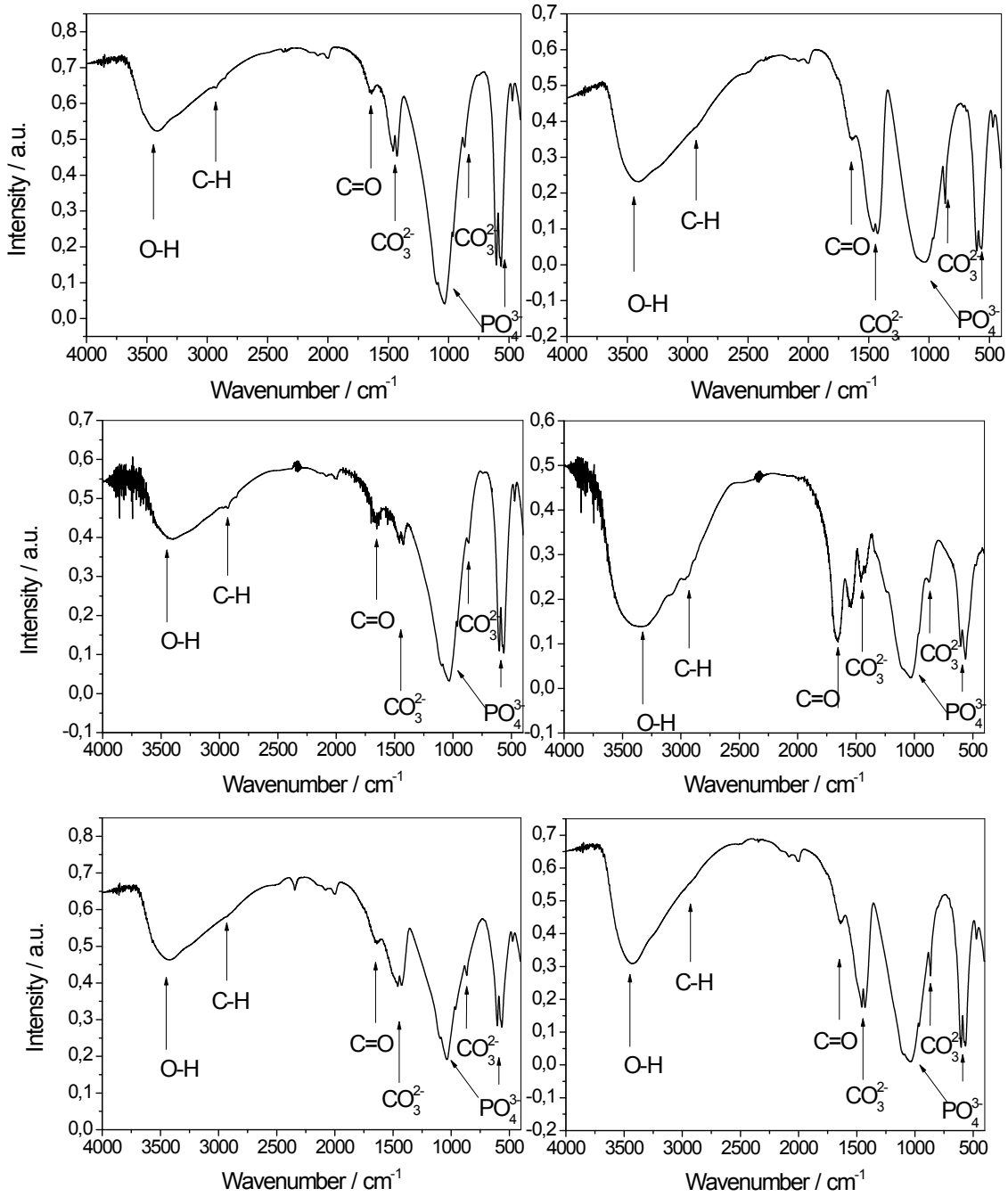

Fig. S18: IR-spectra of the teeth of *C. megalodon* (top), *C. carcharias* (center) and *S. maroccanus* (bottom).

Table 1: Crystallographic properties of enameloid, enamel and dentin of *S. pristodontus, O. obliquus, P. orientalis, C. angustidens, C megalodon, I. hastalis, C. carcharias, S. maroccanus, C. saharicus, P. mauretanicus, M. beaugei*, geological and synthetic hydroxy- and fluoroapatite.

		a-axis / Å	*c*-axis / Å	*V* / Å^3	Domain size / nm
S. pristodontus	Enameloid	9.3782(9)	6.8845(8)	524.4(1)	54
	Dentin	9.350(8)	6.887(6)	521(1)	33
O. obliquus	Enameloid	9.377(1)	6.885(1)	524.2(1)	54
	Dentin	9.374(3)	6.904(2)	525.4(4)	28
P. orientalis	Enameloid	9.3677(3)	6.8813(3)	522.94(4)	57
	Dentin	9.3547(7)	6.8867(6)	521.92(9)	27
C. angustidens	Enameloid	9.3925(3)	6.8971(3)	526.94(4)	63
	Dentin	9.379(4)	6.901(3)	525.7(6)	20
C. megalodon	Enameloid	9.3688(2)	6.8796(2)	522.95(3)	56
	Dentin	9.350(1)	6.887(1)	521.5(1)	17
I. hastalis	Enameloid	9.3954(2)	6.8983(2)	527.35(3)	61
	Dentin	9.377(7)	6.902(5)	525.6(8)	18
C. carcharias	Enameloid	9.401(4)	6.8960(4)	527.81(6)	53
	Dentin	≈ 9.45	≈ 6.87	≈ 531	7
I. oxyrinchus	Enameloid	9.383(1)	6.885(1)	524.9(1)	53
	Dentin	9.403(2)	6.852(2)	524.6(3)	10
G. cuvier	Enameloid	9.387(2)	6.881(2)	525.2(3)	51
	Dentin	9.405(5)	6.832(59	523.4(7)	6
S. maroccanus	Enamel	9.409(4)	6.886(4)	527.99(6)	77
	Dentin	9.376(4)	6.894(4)	524.82(5)	30
C. saharicus	Enamel	9.38(5)	6.89(4)	524.9(6)	38
	Dentin	9.400(4)	6.89(3)	526.7(4)	47
P. mauritanicus	Enamel	9.395(5)	6.887(4)	526.51(6)	52
	Dentin	9.345(6)	6.888(4)	520.98(7)	28
M. beaugei	Enamel	9.411(3)	6.883(2)	527.9(4)	50
	Dentin	9.364(3)	6.900(2)	524.0(4)	29
Geological fluoroapatite single crystal [1]		9.37500(3)	6.88847(3)	524.319(4)	
Synthetic fluoroapatite [2]		9.3716(1)	6.8843(1)	523.62	
Geological hydroxyapatite [3]		9.4249(4)	6.8838(4)	529.56	
Synthetic hydroxyapatite [4]		9.421(6)	6.881(4)	524.13(7)	

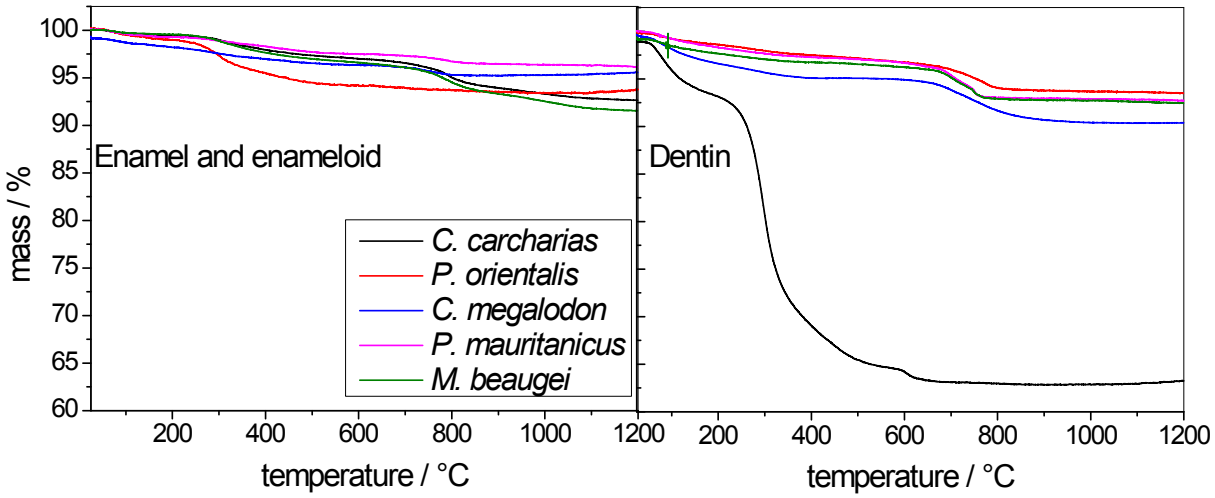

Fig. S19: Thermogravimetry of the teeth of *C. carcharias, P. orientalis, C. megalodon, P. mauritanicus* and *M. beaugei*. The mass losses are given in Table S2.

Table S2: Mass loss during thermogravimetry in wt%.

Species		Release of water, < 200 °C	Combustion of organic material: 200-500 °C	CO_2 release from carbonated apatite > 500 °C	Residual mass (1200 °C)
P. orientalis	Enameloid	1.1	1.7	1.0	96.2
	Dentin	1.5	1.5	3.7	93.3
C. megalodon	Enameloid	0.8	1.6	1.6	96.0
	Dentin	2.9	1.5	4.7	90.9
C. carcharias	Enameloid	1.2	4.5	0.7	93.6
	Dentin	6.2	27.7	2.2	63.9
P. mauretanicus	Enamel	0.6	2.1	4.7	92.6
	Dentin	1.7	1.2	4.4	92.7
M. beaugei	Enamel	0.5	2.6	5.5	91.4
	Dentin	1.7	1.1	4.1	93.1

Table S3: Elemental analysis data by combustion analysis (all data in wt%).

		C	H	N	S
P. orientalis	Enameloid	0.85	0.2	n.d.	0.15
	Dentin	1.25	0.2	n.d.	0.63
C. angustidens	Enameloid	0.79	0.21	n.d.	0.19
	Dentin	2.3	0.51	n.d.	1.34
C. megalodon	Enameloid	0.87	0.31	n.d.	n.d.
	Dentin	1.86	0.37	n.d.	0.98
I. hastalis	Enameloid	0.52	0.12	n.d.	n.d.
	Dentin	1.32	0.31	n.d.	1.26
C. carcharias	Enameloid	2.16	0.48	0.37	0.06
	Dentin	11.2	2.41	3.99	0.1
S. maroccanus	Enamel	1.67	0.3	n.d.	n.d.
	Dentin	1.28	0.21	n.d.	n.d.
C. saharicus	Enamel	2.36	0.4	n.d.	0.41
	Dentin	1.19	0.23	n.d.	0.64
P. mauritanicus	Enamel	1.74	0.31	n.d.	n.d.
	Dentin	1.23	0.19	n.d.	0.63
M. beaugei	Enamel	1.28	0.13	n.d.	0.68
	Dentin	1.6	0.33	n.d.	n.d.

References

1. J. Enax, O. Prymak, D. Raabe and M. Epple, *J. Struct. Biol.*, 2012, **178**, 290-299.
2. L. M. Rodriguez-Lorenzo, J. N. Hart and K. A. Gross, *J. Phys. Chem. B*, 2003, **107**, 8316-8320.
3. A. T. Saenger and W. F. Kuhs, *Z. Kristallogr.*, 1992, **199**, 123-148.
4. O. R. Trautz, *Ann. NY Acad. Sci.*, 1955, **60**, 696-712.